JOURNAL OF APPLIED ELECTROCHEMISTRY 18 (1988) 863–868

Effects of anode–cathode distance on the cell potential and electrical bath resistivity in an aluminium electrolysis cell with a sloping TiB_2 composite cathode

DJEN KASHERMAN, MARIA SKYLLAS-KAZACOS

School of Chemical Engineering and Industrial Chemistry, University of New South Wales, Kensington, N.S.W. 2033, Australia

Received 8 December 1987; revised 8 May 1988

A study of the effects of anode–cathode distance (ACD) on the cell potential and electrical bath resistivity in a laboratory scale cell that utilizes a sloping TiB_2 composite cathode shows an increasing bath resistivity as the ACD decreases, due to a simultaneously increasing gaseous phase fraction in the electrolyte. The effective bath resistivity was found to increase rapidly after ACD = 10 mm and was proportional to the inverse of ACD within this low ACD range studied (2–10 mm). Addition of NaCl to the electrolyte (5.5 wt %) lowered the electrical resistivity by increasing the conductivity of the electrolyte, and at low ACD it also lowered the bubble contribution to the bath resistivity, most likely due to changes in the hydrodynamic properties of the system. Lowering the cryolite ratio (i.e. molar ratio of NaF to AlF_3) resulted in a higher electrical resistivity in the electrolyte by decreasing the conductivity of the melt, as well as by changing the hydrodynamic properties of the melt, leading to an increased bubble contribution to bath resistivity at low ACD. An increase in temperature resulted in a reduced bubble contribution at low ACD in a similar manner as the NaCl addition. From these results, it is clear that for a commercial process, reduction of the ACD and optimization of process conditions to reduce the effect of bubbles should allow significant savings in the energy requirements of the Hall–Heroult process.

1. Introduction

In recent years a considerable amount of work has been carried out to improve the performance of the Hall–Heroult process. One area which has received enormous attention is the utilization of an inert, wettable, drainable cathode material to lower the specific energy consumption and increase the cell life. Two reviews [1, 2] discuss the various works published up to 1981, and they clearly indicate the benefits and problems of using these types of cathodes.

The general requirements for advanced drainable aluminium cell cathode components are: good wettability; low solubility in the metal and electrolyte; good electrical conductivity; cost effectiveness; good thermal shock resistance; good chemical resistance to the electrolyte; good durability, particularly at high temperatures; ease of deployment; ease of fabrication; versatility in the design.

Titanium diboride possesses many of these requirements [3], and is the most promising material to date, although high costs, poor thermal shock resistance and difficulties in fabricating large shapes are still major problems. Its greatest benefits can be realized only when employed in a cell with metal draining facilities. The lower energy consumption is mainly achieved by a lowering of the anode–cathode distance (ACD). In a conventional Hall–Heroult cell, the voltage drop caused by the bath resistance is about 1.8 V or higher, this being due to the high ACD (about 4.5 cm or more) required to prevent short-circuiting of the anode with the mobile aluminium pool that acts as the cathode.

The aim of this study is to investigate the relative effects of varying ACD on the cell potential and bath resistivity in a cell which utilizes a sloping TiB_2 composite cathode. The effects of operating conditions with varying ACD have also been investigated. A study on the effects of ACD has been reported by Doward [4], however the data on bath resistivity at different ACDs cannot be directly extracted due to differences in cathode materials employed, cell design and operating conditions.

2. Experimental details

A series of experimental runs was performed to study the effects of ACD on the cell potential and on the bath resistivity. The following parameters were also investigated in order to check their effects on the effective bath resistivity of the electrolyte (including bubbles): (a) temperature; (b) the effects of CO_2 flowing through the centre of the sloping carbon anode; (c) NaCl addition; (d) cryolite ratio (CR).

The cell was fabricated from a graphite (ATJ grade) crucible, the inside of which was shielded by a recrystallized alumina liner in such a way that only the TiB_2 composite cathode was exposed to the melt. Figure 1

0021-891X/88 $03.00 + .12

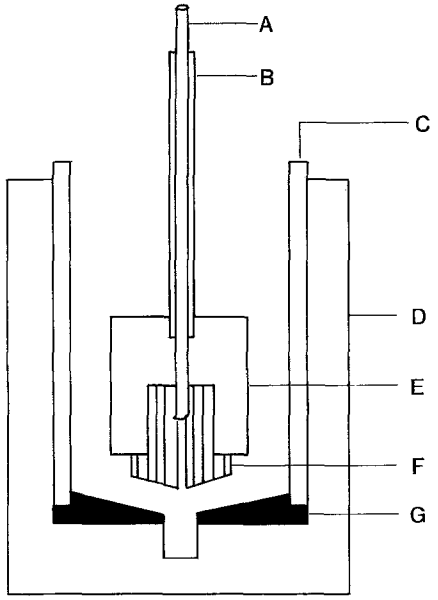

Fig. 1. A schematic diagram of the experimental cell. A = metal rod; B = recrystallized alumina tube; C = recrystallized alumina liner; D = ATJ graphite crucible; E = boron nitride sheath; F = ATJ graphite anode; G = TiB_2 composite cathode.

shows a schematic diagram of the cell, while Fig. 2 shows the design of the second anode employed in this study.

This cell was placed inside an Inconel reactor, and the reactor was positioned such that the cell was in the isothermal zone of a Kanthal resistance furnace. The temperature was maintained constant within $\pm 1°C$. The atmosphere inside the reactor was maintained inert by flushing a stream of purified argon gas. Various electrolyte compositions were employed. The temperature of the electrolyte was measured by means of a chromel–alumel thermocouple, shielded by a closed-end alumina tube (recrystallized grade). The

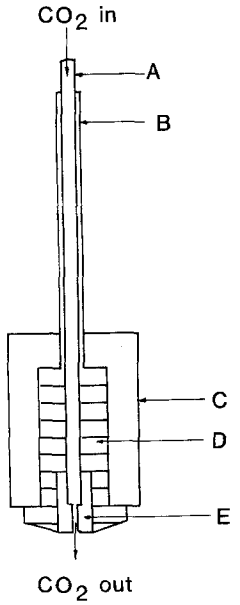

Fig. 2. A schematic diagram of the anode with CO_2 flowing through. A = metal tube; B = recrystallized alumina tube; C = boron nitride sheath; D = ATJ graphite anode; E = boron nitride liner.

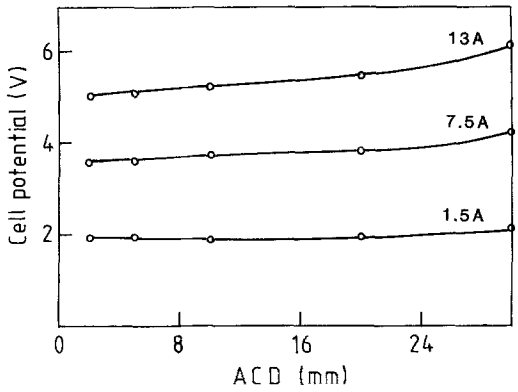

Fig. 3. Cell potential against ACD. $T = 955°C$; CR = 2.35; Al_2O_3 = 7.4 wt %.

height of the electrolyte was about 4 cm, and a crucible lid was employed to minimize vaporization.

The anode (diameter of 30 mm) was fabricated from ATJ graphite material and had the same slope as that of the cathode. The upper section of the anode was covered by a boron nitride sheath to ensure that the geometrically active surface area would be constant at different depths of immersion. The exposed anode surface area was 13.6 cm^2. The cathode was fabricated from a TiB_2/C composite disc attached to the bottom of the cell. The exposed surface area was 34.4 cm^2.

The cell potential data were measured under steady-state galvanostatic conditions for each ACD. Usually about 2 min were required before the cell potential reached a steady-state value. A Hewlett–Packard (HP 6261B) high current d.c. power supply was used in all experimental runs.

3. Result and discussion

The effects of varying ACD can be observed from Fig. 3 which shows the cell potential against ACD at various current densities, in an electrolyte which had an alumina concentration of 7.4 wt %, CR = 2.35, 1.83 g of aluminium. A temperature of 955° C was employed. The trend indicates that the reduction in voltage with decreasing ACD is not as much as would be expected in a normal case in the absence of bubbles.

The cell voltage, V_{cell}, consists of a number of contributions as indicated in Equation 1 below

$$V_{cell} = V_N + \eta_{ar} + \eta_{ac} + \eta_{cr} + \eta_{cc} + IR_e + IR_b + \Sigma V_i \quad (1)$$

where

V_N = The minimum potential required to produce Al and CO_2. Using the method described by Haupin [6] and thermodynamic data from JANAF Tables [7], V_N values of 1.195, 1.186 and 1.178 V were calculated for temperatures 955, 970 and 985° C, respectively.

η_{ar} = Anodic reaction overvoltage which is the extra potential required to maintain the reaction rate. Within a typical set of operating conditions, this generally obeys Tafel behaviour

Table 1. Bath resistivity and conductivity values from Ref. [5]

Conditions	*Specific conductivity* $\tau\ (\Omega\,cm)^{-1}$	*Bath resistivity* $\Gamma\ (\Omega\,cm)$
CR = 2.35, Al_2O_3 = 7.4 wt % T = 955° C	1.9919	0.50205
CR = 2.35, Al_2O_3 = 7.4 wt %, T = 970° C	2.0327	0.49195
CR = 3.0, Al_2O_3 = 7.5 wt %, T = 985° C	2.3833	0.41948
CR = 3.0, Al_2O_3 = 7.5 wt %, T = 985° C, NaCl = 5.5 wt %	2.4674	0.40529
CR = 2.13, Al_2O_3 = 7.5 wt % T = 985° C, NaCl = 5.5 wt %	2.0421	0.4897

The values are obtained from the equation below:

$$\ln(\tau) = 2.0156 - 0.0207[Al_2O_3] - 0.005[CaF_2] - 0.0166[MgF_2] + 0.0178[LiF] + 0.0077[Li_3AlF_6] + 0.0063[NaCl] + 0.4349BR - 2068.4/T$$

τ is in $(\Omega\,cm)^{-1}$, T is in K, [ ] is concentration in wt %, and BR or bath ratio is weight ratio of NaF against AlF_3, approximately equal to CR/2.

[2, 5, 6], represented by the following equation:

$$\eta_{ar} = \frac{RT}{\alpha nF} \ln (i/i_0) \qquad (2)$$

Using the published values for the reaction order, α, and exchange current density i_0 for graphite [8], at T = 955° C, a value of 0.53 V was calculated for η_{ar}. For T = 970° C, η_{ar} is 0.50 V, while for T = 985° C, η_{ar} is 0.48 V.

η_{ac} = Anodic concentration overvoltage, which is caused by depletion of reacting species from the surface of the electrode. In an alumina saturated melt, and for the current density employed, this overvoltage is close to zero, and can therefore be neglected [2, 5, 6, 9].

η_{cr} = Cathodic reaction overvoltage which has also been found to be negligible [2, 5, 7].

η_{cc} = Cathodic concentration overvoltage which is due to the concentration gradients existing in the cathode layer. Using the correlation described by Haupin [6], the following overvoltage values were calculated:
for CR = 2.35, η_{cc} = 0.034 V at T = 955–970° C.
for T = 985° C, values of 0.032 and 0.035 V were obtained at CR = 3.0 and 2.13, respectively.

IR_e = The ohmic drop caused by electrolyte resistivity. This is dependent on the specific conductivity of the electrolyte as outlined in Table 1 for various operating conditions.

IR_b = Ohmic drop caused by bubbles present near the surface of the anode, and also in the bath.

ΣV_i = Total voltage drops due to resistance of the conductors etc.

When ACD is varied at a constant current density, the components of the cell potential that vary are the ohmic drops across the electrolyte, IR_e, and the CO_2 bubble layer, IR_b, all other terms remaining constant.

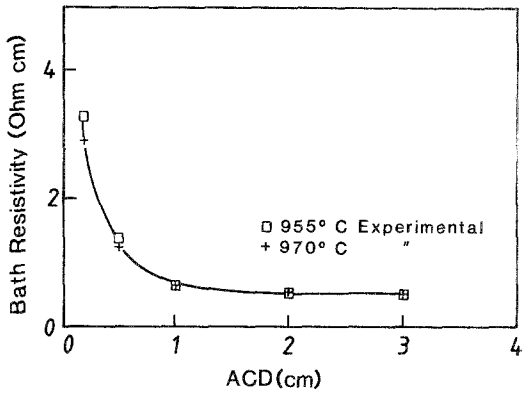

Fig. 4. Bath resistivity against ACD. T = 955° C; CR = 2.35; Al_2O_3 = 7.4 wt % and T = 970° C; CR = 2.35; Al_2O_3 = 7.4 wt %.

Using the V_{cell} data and the above assumptions the values of $(IR_e + IR_b)$ were calculated for different conditions. The sum of IR_e and IR_b represents the effective bath resistivity Γ (i.e. resistivity of the bath and bubble layer as described by the following equation:

$$(IR_e + IR_b) = \Gamma i \mathrm{ACD} \qquad (3)$$

where

Γ = effective bath resistivity (Ω cm)

i = anode current density (A cm^{-2})

ACD = anode–cathode distance (cm).

From this equation and the cell potential data, the bath resistivity was calculated at each ACD. The bath resistivity at the highest ACD (i.e. 3 cm) was found to be close to the theoretical value listed in Table 1 for any operating conditions. It is expected that at this ACD, the contribution of the bubbles to bath resistivity is negligible. Any differences in magnitude are associated with the random errors of measurements.

In the above calculations, it has been assumed that the current density remains constant with varying ACD. Because of the cell geometry, however, changes in current distribution, mainly associated with the vertical surface area of the anode, would mean a

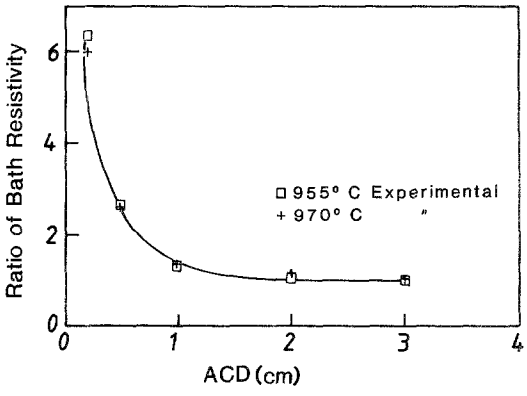

Fig. 5. Ratio of bath resistivity against ACD. T = 955° C; CR = 2.35; Al_2O_3 = 7.4 wt % and T = 970° C; CR = 2.35; Al_2O_3 = 7.4 wt %.

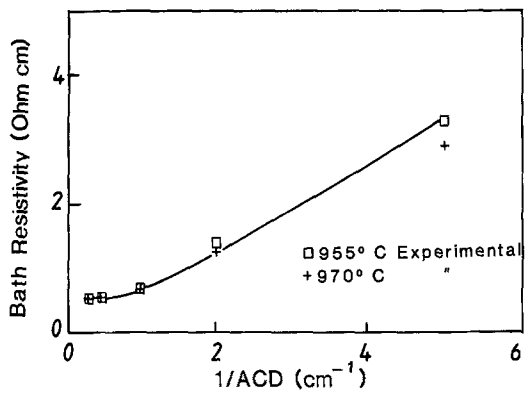

Fig. 6. Bath resistivity against 1/ACD. T = 955° C; CR = 2.35; Al_2O_3 = 7.4 wt %.

reduction in the fraction of current passing through this area as the ACD is decreased. The changes in current distribution with varying ACD are complex to calculate, particularly since the presence of bubbles leads to further complications. The above changes in current distribution will therefore affect the values of bath resistivity calculated, however the trends obtained for different operating conditions will not be affected since the same cell geometry was used in all experiments. A mathematical analysis of the current distribution will be presented in a future publication.

The values of bath resistivity at each ACD were normalized with respect to the highest ACD so as to further study the effects of bubbles with decreasing ACD. The highest ACD in this experiment was 30 mm, thus the bath resistivity value at ACD = 30 mm was used to obtain the ratio of bath resistivities for each experiment.

For an ideal case, where there is no effect of bubbles on bath resistivity, a constant ratio of 1 would be expected at any ACD. A ratio greater than 1 would be indicative of increasing contribution of the bubble layer on the bath resistivity [4].

Figures 4 and 5 show that the values of bath resistivity and the ratio Γ/Γ_{30} (at 1 A cm^{-2}) do in fact increase as ACD decreases. This clearly illustrates the increasing effect of bubbles on bath resistivity which is due to increasing gas phase volume fraction of the bubbles in the electrolyte [4] as ACD is decreased.

Plotting the values of bath resistivity and the ratio Γ/Γ_{30} against 1/ACD, as in Figs 6 and 7, shows a linear

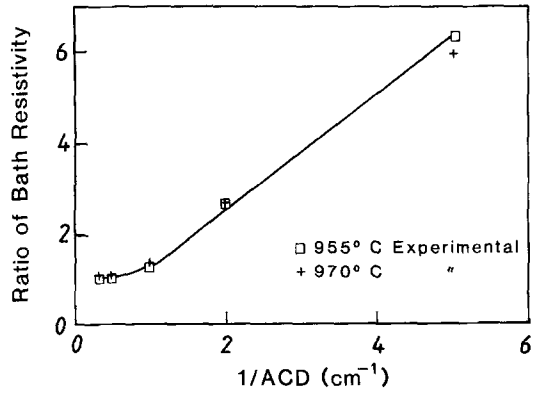

Fig. 7. Ratio of bath resistivity against 1/ACD. T = 955° C; CR = 2.35; Al_2O_3 = 7.4 wt %.

Table 2. Bath resistivity (Ω cm)

ACD (mm)	*Conditions*		
	No CO_2	*T = 970° C No CO_2*	*With CO_2 Flow rate = 79 ml min^{-1}*
2	3.29	2.90	4.05
5	1.38	1.24	1.72
10	0.66	0.68	1.02
20	0.53	0.54	0.73
30	0.52	0.48	0.65

Al_2O_3 = 7.4 wt %, T = 955° C unless indicated, CR = 2.35.

relationship over the low ACD range (2–10 mm). At very large ACDs, however, the effect of the bubbles on bath resistivity would become negligible, so that the resistivity would approach a constant value. A slight deviation from linearity is in fact observed at low 1/ACD values in Figs 6 and 7 as constant resistivity is approached. At very low ACD, or for higher 1/ACD values than those studied, the bath resistivity values would be expected to increase rapidly as the gas phase volume fraction approaches 1 and the bubbles insulate the electrode from the bath. Tables 2 and 3 summarize the experimental values of bath resistivities and ratio Γ/Γ_{30} at different ACDs for the various operating conditions employed in this study.

3.1. *Effects of temperature*

When the temperature was increased to 970° C, the cell potentials decreased as expected, although the trends were the same as those at the lower temperature. Direct comparison of bath resistivity values (at any ACD) indicates a reduction in bath resistivity (Fig. 4). A comparison of the Γ/Γ_{30} ratios however shows similar values at high ACDs (Fig. 5), but significant differences at low ACDs. It can thus be concluded that increasing the temperature not only reduces bath resistivity by increasing conductivity (refer to Table 1), but also reduces the bubble resistive component at low ACDs. A lower viscosity of the melt at higher temperature alters the hydrodynamic properties of the electrolyte, and may explain the reduced effects of the bubbles at the lower ACDs.

Table 3. Ratio of bath resistivity, ACD = 30 mm as base

ACD (mm)	*Conditions*		
	No CO_2	*T = 970° C No CO_2*	*With CO_2 Flow rate = 79 ml min^{-1}*
2	6.34	5.99	6.20
5	2.65	2.56	2.63
10	1.27	1.40	1.57
20	1.02	1.11	1.12
30	1.00	1.00	1.00

Al_2O_3 = 7.4 wt %, T = 955° C unless indicated, CR = 2.35.

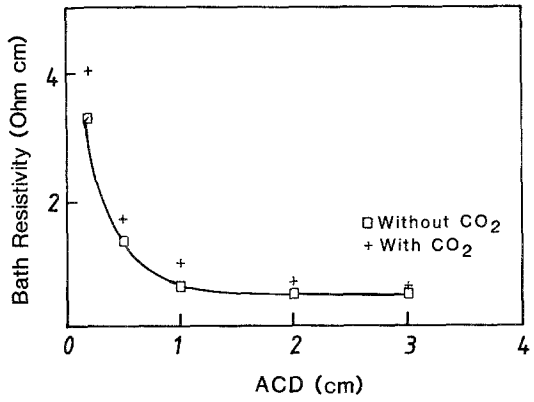

Fig. 8. Bath resistivity against ACD. T = 955°C; CR = 2.35; Al_2O_3 = 7.4 wt %; CO_2 flow rate = 117 ml min^{-1} at NTP.

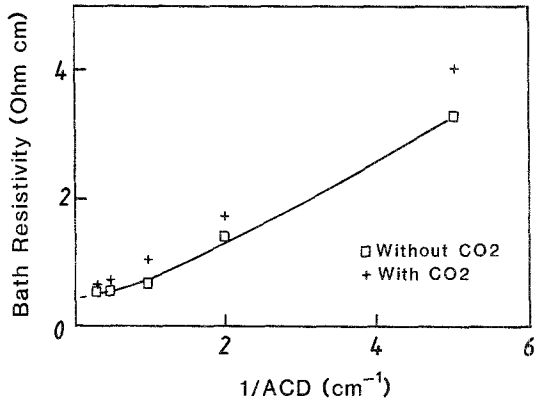

Fig. 10. Bath resistivity against 1/ACD. T = 955°C; CR = 2.35; Al_2O_3 = 7.4 wt %; CO_2 flow rate = 117 ml min^{-1} at NTP.

3.2. *Effects of using C/CO_2 sloping anode*

The small size of the anode used in this study may hinder the formation of large bubbles by providing an easier escape route thereby resulting in lower bubble resistivities than in larger cells. A second anode design was thus employed to investigate the effects of the presence of more CO_2 bubbles in the cell. This electrode had an inert boron nitride section in the centre to allow CO_2 gas to flow through (Fig. 2). The inner BN liner was employed so as to prevent reaction between the CO_2 gas and the anode carbon material.

Results obtained with this electrode showed similar trends to those obtained with the first anode (no CO_2 flowing). The bath resistivity values and the ratio Γ/Γ_{30} were calculated and plotted against ACD, in Figs 8 and 9, and also plotted against 1/ACD in Figs 10 and 11.

Comparing these results with those obtained using the simple anode indicates a big increase in the bath resistivity values, but for the ratio Γ/Γ_{30} values, no significant differences can be observed. The increase in bath resistivity is believed to be caused by the thicker bubble layer when there is CO_2 flowing through the anode, which consequently become significant enough to cause deviation from the predicted value. From Figs 8 and 9, it can be observed that the rapid deviation (increase) of bath resistivity when using the second anode occurs at higher ACD than that with the first electrode indicating a thicker bubble layer.

From Figs 10 and 11, the Γ/Γ_{30} ratio values show that there is no increased bubble contribution in the presence of more bubbles, since the Γ/Γ_{30} values with or without injected CO_2 gas through the electrode show similar magnitudes.

The carbon dioxide gas flow rate was varied between 79 and 132 ml min^{-1} (NTP), but as shown in Table 4 no effect on the bath resistivity values could be observed in this range. Lower CO_2 flow rate could not be employed because of technical difficulties.

3.3. *Effects of NaCl addition*

NaCl (concentration of 5.5 wt % of the melt) was added to the electrolyte which had an alumina concentration of 7.5 wt % and CR = 3.0 (no correlation was made for the presence of NaCl).

The values of bath resistivity and ratio Γ/Γ_{30} obtained for this melt at 985°C again showed the same trends as before. Comparing the results obtained in melts with and without NaCl (Tables 5 and 6, columns 2 and 3) shows that the presence of NaCl significantly lowers the bath resistivity values, due to the increased bath conductivity (Table 1).

The value of the ratio Γ/Γ_{30} at low ACD (2 mm) however is lower, suggesting an alteration in the hydrodynamic properties of the melt, such as the surface

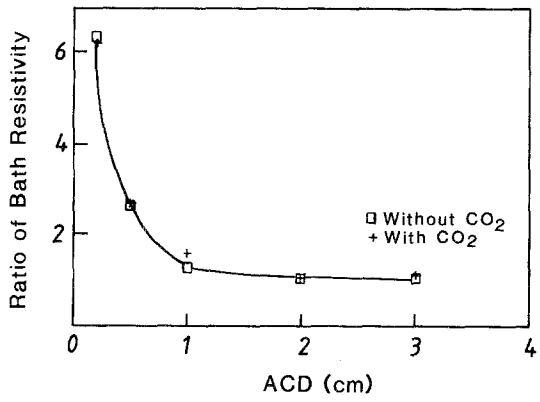

Fig. 9. Ratio of bath resistivity against ACD. T = 955°C; CR = 2.35; Al_2O_3 = 7.4 wt %; CO_2 flow rate = 117 ml min^{-1} at NTP.

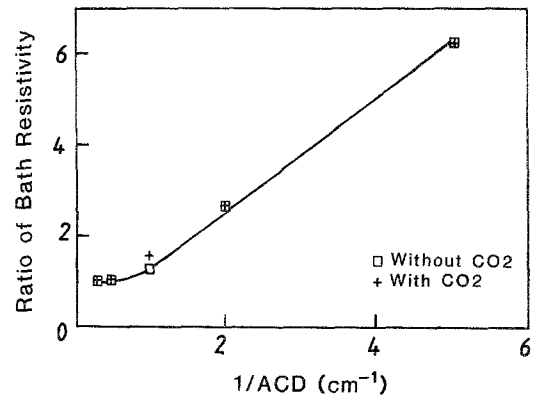

Fig. 11. Ratio of bath resistivity against 1/ACD. T = 955°C; CR = 2.35; Al_2O_3 = 7.4 wt %; CO_2 flow rate = 117 ml min^{-1} at NTP.

Table 4. Effects of CO_2 flushing on bath resistivity

CO_2 flow rate ($ml\,min^{-1}$)	Bath resistivity ($\Omega\,cm$)	
	ACD = 10 mm	*ACD = 5 mm*
No CO_2	0.657	1.375
79	1.024	1.718
113	1.020	1.725
132	1.025	1.720

Conditions: CR = 2.35, T = 955° C, Al_2O_3 = 7.4 wt %.

tension or viscosity, so that bubbles may find it easier to escape. This phenomenon is only noticed at very low ACD because of the small bubbles produced by the very dense ATJ graphite carbon anode, the small size of the anode and the short electrolysis time. In the real Hall–Heroult environment, the bubble sizes will be much larger and the bubble layer thickness greater due to larger anode and more porous baked carbon material used industrially.

Tables 5 and 6 summarize the calculated bath resistivity and the ratio Γ/Γ_{30} values showing the effects of NaCl addition and CR variation.

3.4. *Effects of CR*

AlF_3 was added to the above melt to study the effect of varying CR. It was expected that the lower CR (2.13) would lower conductivity and therefore would increase the resistivity (refer to Table 1).

The results shown in Tables 5 and 6 (comparing column 3 with column 4) do indicate a significant rise in bath resistivity values. At low ACD (2 mm) however, a greater increase in the ratio Γ/Γ_{30} is observed, showing an increase in the bubble contribution on the bath resistivity. The hydrodynamic properties of the melt (i.e. the surface tension or viscosity) appear to have been altered by the changing cryolite ratio.

4. Conclusions

The results from the present study of bath resistivities in a cell with sloping TiB_2 composite cathode and sloping ATJ carbon anode show that as ACD decreases, the bath resistivity increases because of the increased contribution from bubbles, as shown by an increase in the ratio Γ/Γ_{30}. At ACD lower than 10 mm, the bath resistivity increases rapidly, and within the range 2–10 mm, bath resistivity and also Γ/Γ_{30} ratio are inversely proportional to 1/ACD. The experimental bath resistivity values at ACD = 30 mm are in very good agreement with the literature values as listed in Table 1.

Table 5. Bath resistivity ($\Omega\,cm$)

ACD (mm)	*Conditions*		
	CR = 3.0 No NaCl	*CR = 3.0 NaCl = 5.5 wt %*	*CR = 2.13 NaCl = 5.5 wt %*
2	3.54	2.89	3.65
5	1.52	1.40	1.59
10	0.84	0.79	0.84
20	0.52	0.47	0.50
30	0.42	0.38	0.41

T = 985° C, Al_2O_3 = 7.5 wt %.

Table 6. Ratio of bath resistivity, ACD = 30 mm as base

ACD (mm)	*Conditions*		
	CR = 3.0 No NaCl	*CR = 3.0 NaCl = 5.5 wt %*	*CR = 2.13 NaCl = 5.5 wt %*
2	8.50	7.54	8.89
5	3.64	3.64	3.86
10	2.03	2.07	2.04
20	1.25	1.23	1.22
30	1.00	1.00	1.00

T = 985° C, Al_2O_3 = 7.5 wt %.

Addition of NaCl reduces bath resistivity values, and at low ACD a reduction of bubble effects is encountered. Lowering CR, however, increases the bath resistivity and at low ACD also increases the bubble contribution to the bath resistivity. A higher temperature also results in decreased bath resistivity values and, at low ACD, a reduction of bubble effects is observed.

The above results suggest that a reduction in the bubble contribution to the bath resistivity can be achieved by altering the hydrodynamic properties (surface tension and viscosity) of the electrolyte, thus making it possible to reduce the ACD considerably in an aluminium electrolysis cell employing a sloping TiB_2 cathode and a sloping anode. Although the use of a graphite anode does not permit direct comparison with an industrial cell, similar trends would be expected with a carbon anode.

Acknowledgement

This research work has been funded by a grant from COMALCO Ltd. The authors are grateful to COMALCO for permission to publish these results and for the supply of some of the special materials used. The useful discussions with B. J. Welch and G. J. Houston are also greatly appreciated.

References

[1] K. Billehaug and H. A. Øye, *Aluminium* **56** (1980) 642, 713.
[2] K. Grjotheim, C. Krohn, M. Malinovsky, K. Matiasovsky and J. Thonstad, 'Aluminium Electrolysis', Aluminium Verlag GmbH, Dusseldorf (1982).
[3] K. W. Tucker, J. T. Gee, J. R. Shaner, L. A. Joo, A. T. Tabereaux, D. V. Stewart and N. E. Richards, *Light Metals* (1987) 345.
[4] R. C. Doward, *J. Appl. Electrochem.* **13** (1983) 569.
[5] K. Grjotheim and B. J. Welch, 'Aluminium Smelter Technology'. Aluminium Verlag GmbH, Dusseldorf (1980).
[6] W. E. Haupin and W. B. Frank, in 'Comprehensive Treatise of Electrochemistry' (edited by J. O'M. Bockris *et al.*). Plenum, New York (1981) Vol. 2, Ch. 5, p. 301.
[7] JANAF Thermochemical Tables (1965).
[8] J. Thonstad, *Electrochim. Acta* **15** (1970) 1569.
[9] R. Piontelli, B. Mazza and P. Pedeferri, *Electrochim. Acta* **10** (1965) 1117.